11th International Symposium on Turbulence and Shear Flow Phenomena (TSFP11)
Southampton, UK, July 30 to August 2, 2019

A COMPUTATIONAL AND EXPERIMENTAL STUDY OF PHYSIOLOGICAL PULSATILE FLOW IN AN AORTIC ANEURYSM

M.Bopp, A.Bauer, S.Wegt, S.Jakirlic and C.Tropea
Institute of Fluid Mechanics and Aerodynamics, Technische Universität Darmstadt
Alarich-Weiss-Straße 10, 64287 Darmstadt, Germany
bopp, bauer, wegt, jakirlic, tropea@sla.tu-darmstadt.de

A.Krafft, N.Shokina and J.Hennig
Department of Radiology, University of Freiburg
Breisacher Straße 60a, 79106 Freiburg, Germany
axel.krafft, nina.shokina, juergen.hennig@uniklinik-freiburg.de

ABSTRACT

The present study is concerned with numerical simulations and experiments of the pulsatile flow in a generic aortic aneurysm model. The flow rate variation in time follows closely a realistic physiological blood circulation pulse. The maximum Reynolds number achieved under the human resting conditions corresponds approximately to 3200. After reaching the maximum volume flow rate, the flow is decelerated until it reverses its direction. Then a second, weaker flow acceleration reverses the flow again into the main flow direction. The main objective of the study is the estimation of the time-resolved hemodynamic wall shear stress, representing a parameter of importance for risk estimation of aorta aneurysm rupture. Initially, experimental investigations of a stationary flow in a similar Reynolds number range have been performed using Magnetic Resonance Velocimetry (MRV), Bauer *et al.* (2019). The MRV provides three-dimensional, three-component velocity fields, which serve as a basis for the wall shear stress estimation. Accompanying numerical simulations employ three different turbulence models - baseline, transition-sensitive and eddy-resolving models, all based on a near-wall second-moment closure formulation. In accordance with the relatively low Reynolds number range, pure laminar computations have also been performed. The investigated flow configuration exhibits a transitional, low-intensity turbulent behaviour. The temporal and spatial evolution of the experimentally and numerically obtained wall shear stress shows a high level of correspondence over the entire cardiac cycle.

INTRODUCTION

The human cardiovascular system provides an array of elastic conduits in which a cyclic blood flow is driven by the periodically beating heart. Apart from supplying organs and surrounding tissue with oxygen, nutrients and hormones it is responsible for the removal of emerging metabolic products. The cardiovascular system is therefor divided in two main circulations, the pulmonary and the systemic circulation. The pulmonary circulation, including the lungs, ensures the oxygenation of red blood cells within the circulating blood flow. The systemic circulation then provides the oxygenated blood to the rest of the body, supplying all vital organs and tissues. The oxygenated blood enters the systemic circulation by leaving the left ventricle of the heart through the aortic semilunar valve into the largest artery of the human body. This main artery, the so called aorta, is extending through the whole thorax down to the caudal ending of the abdomen with a diameter of up to 26 mm (Mao *et al.*, 2008). The pulsatile nature of the blood flow,

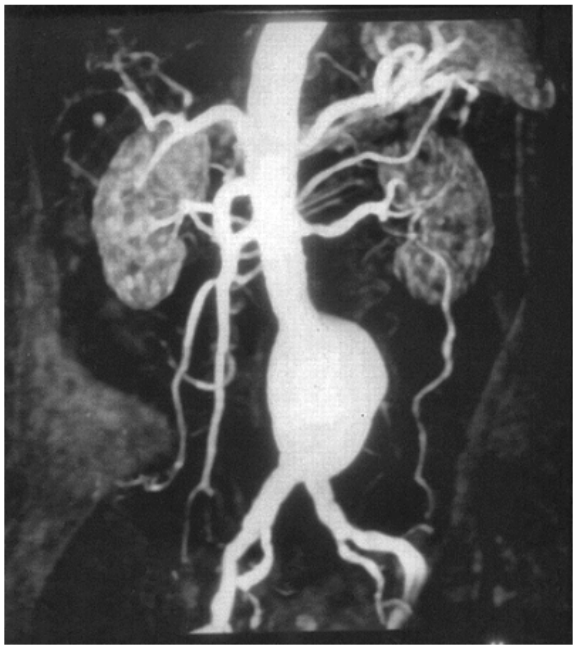

Figure 1. Magnetic Resonance Angiography (MRA) of an abdominal aortic aneurysm. (Kaufman *et al.*, 1994)

which is imprinted by the contraction of the cardiac muscle, leads to periodically arising hemodynamic stresses on the aortic vascular walls. In case of a healthy individual, the tissue of vascular walls is constantly renewed to ensure suf-

ficient elasticity to withstand the emerging periodic loads. Individual risk factors like weak connective tissue or hypertension can lead to pathophysiological processes, which result in degenerative changes of the aortic blood vessel (Lasheras, 2007). These degenerative changes may impair elasticity and increase the surface roughness of the blood vessel. It is well accepted that particularly hemodynamic normal and wall shear stresses (WSS) are major mechanical factors, which promote elastic degeneration and eventually lead to a bulging of the arterial wall. This bulging can lead to a dangerous degenerative condition which manifests itself in form of a localized enlargement of the abdominal aorta, a so called abdominal aortic aneurysm (AAA) (Fig 1). If an AAA reaches an individual critical diameter, the probability of a rupture increases rapidly. Once it is ruptured, the affected person is in life-threatening danger and requires an immediate medical surgery. Due to the severe internal blood loss, caused by a ruptured AAA, the mortality rate is at 90%. To reduce the threat of an AAA and to treat affected patients correctly, a comprehensive understanding of the corresponding pathogenesis is indispensable. As previously mentioned, the hemodynamic WSS is identified as a main mechanical factor for the development and growth of an AAA. A measurement of this WSS could provide the key for a better understanding of the pathological processes. However, it is problematic to observe emerging wall shear stresses in the interior of a closed aortic blood vessel. The most promising results in this field have been obtained by a non-invasive measurement technique named Magnetic Resonance Velocimetry (MRV). It can capture three-dimensional velocity field data and does not expose the patients to any high-energy radiation. The fact that the sought-after wall shear stress is directly proportional to the wall-normal velocity gradient, allows a calculation from the MRV velocity field data. Unfortunately, the main limitation of MRV while using reasonable measurement times is the low spatial resolution, typically in the order of a cube with an edge length of 1 mm. This circumstance can result in an underprediction of the WSS, leading to errors of up to 40% (Petersson *et al.*, 2012). To improve the MRV measurement technique, a reference database replicating the flow conditions of aortic aneurysms is necessary. However, comparable literature data is rarely available. This circumstance motivates the present computational work on a physiologically pulsating flow in a generic AAA model. The computational investigation is carried out with three Unsteady RANS models with respectively different strengths. All URANS models are based on a second-moment closure formulation using a transport equation governing the dynamics of the Reynolds stress tensor. The obtained computational database enables an in-depth analysis of the flow structure along with the MRV data.

FLOW CONFIGURATION DESCRIPTION

The human aorta has a complex, patient specific geometry. Its pathway and geometry varies strongly between different individuals. The diverse anatomic nature of the aorta prevents a clear formulation for generic experiments or analytically accessible flow conditions ((Bauer *et al.*, 2019)). The goal of the current investigation is the development of experimental and numerical techniques to obtain a ground truth for a simplified, generic abdominal aortic aneurysm. Therefore, the geometry of a generic aneurysm model based upon the work of Vorp *et al.* (1998) is used. The geometry consists of a generic healthy aortic blood vessel with an undistorted diameter of d = 26 mm leading in to an axis-symmetric generic aneurysm with a maximum diameter of D = 65 mm and a length of L = 104 mm (corresponding to L/d= 4 and D/d = 2.5). Figure 2 shows the geometry of the generic AAA model with typical velocity profiles of a pulsating aneurysm flow. The temporal evolution of the volume flow rate (Fig. 2, bottom) corresponds to realistic flow conditions within a human aorta. The physiologically pulsating flow, taken from Salsac *et al.* (2006), starts with a strong flow acceleration in the beginning, reaching a maximum Reynolds number of 3200 after 0.5 seconds. After reaching the maximum volume flow rate, the flow is decelerated until it reverses its direction, developing a short period of a back flow after 1.4 seconds. Then the second flow acceleration reverses the flow direction again, forming a second positive volume flow rate peak after 1.7 seconds. All experiments and computations are conducted at the same dimensionless frequency of the flow, which in biomedical flows is expressed via the Womersley number $Wo = R\sqrt{\omega/\nu}$, where R is the pipe radius, ω the angular frequency and ν the kinematic viscosity coefficient (Womersley, 1955).

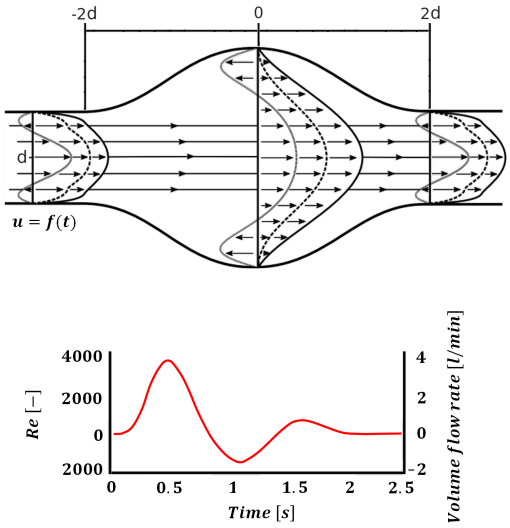

Figure 2. Pulsating flow through a generic aneurysm. ((Bauer *et al.*, 2019))

EXPERIMENTAL METHODOLOGY

This section describes the experimental setup and the used measurement technique. Figure 3 shows the schematic experimental setup which extends over two separated rooms. Due to the strong magnetic field of the MRI scanner, it is necessary to relocate the experiment controls into a separate room. The working fluid for the experiments is water, which is doped with copper sulfate as a contrast agent to increase the signal-to-noise ratio (SNR). The flow supply system controls the volume flow rate with a stepper motor driven gear pump. Downstream of the pump, the flow passes through a high precision Coriolis flow meter to measure the volume flow rate. To ensure fully-developed flow conditions at the measurement section, several precautions are taken. First, all upstream disturbances caused by bends

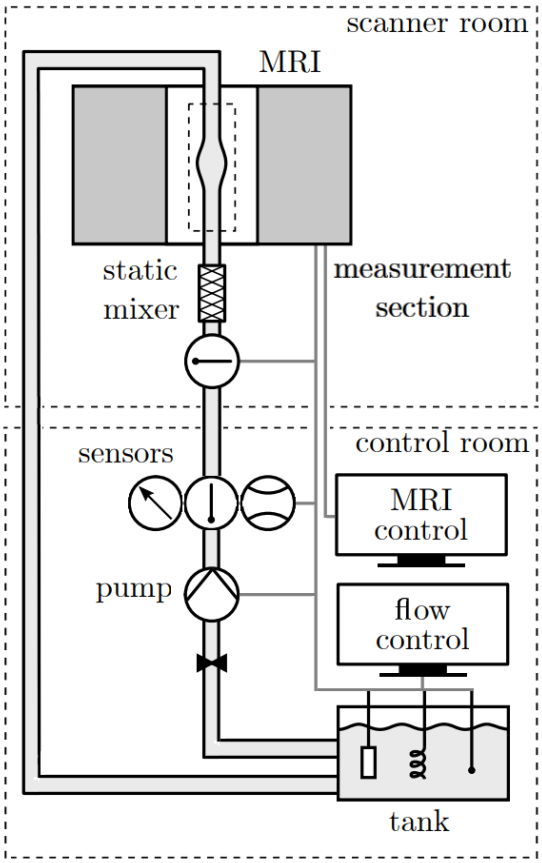

Figure 3. Experimental setup in two separate rooms, taken from the work of (Bauer *et al.*, 2019).

are eliminated with a static mixer. Afterwards an acrylic tube of 26 mm inner diameter and l = 2m length is used as an inlet, corresponding to l/d = 77. Special caution is taken with regard to secondary flow motion, which might occur when a temperature difference between ambient and fluid is present. Heat exchange is avoided by insulating the pipe thermally and matching the inner and outer temperature. Dissolved gases within the water were removed with a vacuum pump. The measurement section consists of the aneurysm model, which is made of polyamide and is manufactured by using laser powder bed fusion. Downstream of the measurement section a straight outflow of 0.5 m length is used ((Bauer *et al.*, 2019)). The Magnetic Resonance Velocimetry is capable of obtaining three-dimensional, time-resolved velocity fields inside the closed aneurysm geometry. The MRV experiments for the present work are carried out at the Department of Radiology at the University of Freiburg using a 3 Tesla whole-body scanner (MAGNETOM Prisma, Siemens Healthcare, Erlangen, Germany). The MRV data is acquired with a phase-contrast 4D-Flow sequence applied to the 3 Tesla Siemens Prisma unit. Three velocity components are obtained over a three-dimensional volume with a spatial resolution of 0.6 mm. The phase-averaged measurements include 36 time steps over the cardiac cycle, corresponding to a temporal resolution of 72.8 *ms*. The result of this measurement technique is a temporally evolving three-dimensional raster graphic. The 3D image volumes of this raster graphic are called voxel and contain the information of a velocity vector. For better understanding, a voxel can be described as the three dimensional counterpart to a pixel of a 2D raster graphic. The measured velocity fields can be used to postprocess the WSS on the contact surface of the measurement fluid and the inside solid aneurysm boundary. The WSS is calculated by using the viscous stress law reading:

$$\tau_W = \rho \nu \frac{\partial u_{tan}}{\partial n}\bigg|_{n=0} \tag{1}$$

The WSS τ_W depends on the kinematic viscosity ν, the density of the fluid ρ and the wall normal velocity gradient $\partial u_{tan}/\partial n$. The limited spatial resolution and finite number of voxels can lead to errors in WSS approximation. The computational study employing some advanced turbulence models (see next section) provided a detailed flow field enriching appropriately, in addition to the MRV data, the comprehensiveness of its temporally and spatially resolved structural properties.

COMPUTATIONAL METHODOLOGY

The turbulence model equations are implemented into the finite-volume-based open source toolbox OpenFOAM®(Open Source Field Operation and Manipulation) with which all calculations are performed. The numerical calculations of the pulsating aneurysm flow, characterized by a weakly turbulent regime (known as 'turbulescence'), are performed using Reynolds-Averaged Navier-Stokes (RANS) models. A controlled adaptive time step ensures a Courant number $Co = u\Delta t/\Delta x$ smaller than 1 for the entire solution domain. The discretization of the convective terms is performed by applying the well-known deferred correction approach, blending appropriately between the Central Differencing Scheme (CDS) and the Upwind-type Scheme. The flow domain is meshed by

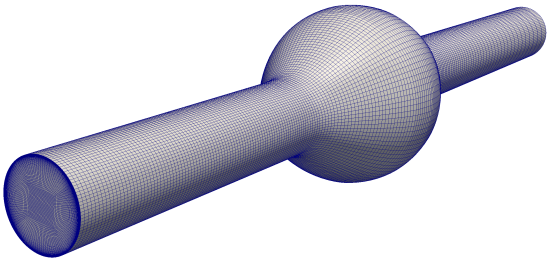

Figure 4. Three-dimensional mesh arrangement of the generic aortic aneurysm configuration.

using the open source toolbox OpenFOAM®and its mesh utility denoted as 'blockMesh'. The generic aneurysm geometry is meshed with a structured, three-dimensional, fully hexahedral grid consisting of 1.18 million cells in total. A grading towards the walls, ensures that the wall-next computational node is located well within the viscous sublayer, exhibiting a dimensionless wall distance y^+ substantially smaller than one for the entire simulation time. To avoid retroactive effects the inlet and outlet of the solution domain are located five hydraulic diameters away from the beginning and the end of the actual aneurysm.

Turbulence modelling

The computational study focuses on the performance of three RANS models with respectively different strengths. All presently applied RANS models are formulated within the second-moment closure modelling framework based on the following equation governing the Reynolds stress tensor $\overline{u_i'u_j'}$:

$$\frac{D\overline{u_i'u_j'}}{Dt} = P_{ij} + \Phi_{ij} - \varepsilon_{ij}^h + \left(0.5D_{ij}^{\nu} + D_{ij}^{p'} + D_{ij}^{u'}\right) \qquad (2)$$

As is well known, the terms Φ_{ij}, ε_{ij}^h, $D_{ij}^{u'}$ and $D_{ij}^{p'}$, representing the stress redistribution, stress dissipation, turbulent and pressure diffusion transports respectively, must be further modelled, whereas the Reynolds stress production P_{ij} and the viscous diffusion $D_{ij}^{\nu'}$ can be exactly treated. For the sake of brevity the detailed model specification will be not presented here; interested readers are referred to Jakirlić & Hanjalić (2002), Jakirlić & Maduta (2015) and Jakirlić & Maduta (2016). All presently used models utilize homogeneous part of the inverse time scale - $\omega^h = \varepsilon^h/k$ (with $\varepsilon^h = 0.5\varepsilon_{ii}^h$ and $k = 0.5\overline{u_i'u_i'}$), representing the model's scale-supplying variable.

The first model is a conventional RANS model satisfying the exact asymptotic behaviour of all Reynolds stress components by approaching the solid wall as well as a correct near-wall profile shape of the dissipation rate of the turbulence kinetic energy k. Accordingly, the model is capable of capturing correctly not only the strengthen viscosity effects, but also both Reynolds stress and stress dissipation anisotropies. This Reynolds-Stress Model (RSM) acts as the baseline model version underlying the other two RANS-RSM models used presently: the transition-sensitive RSM, denoted as 'kkLOmegaRSM' and its eddy-resolving counterpart IIS-RSM (Improved Instability-Sensitive Reynolds Stress Model). The transition-sensitive modelling approach is based on blending the relevant source terms in the momentum and Reynolds stress equations, with those originating from an appropriately modified eddy-viscosity-based model governing the pre-turbulent kinetic energy. The correspondingly blended Reynolds stress formulation is written as followed:

$$\overline{u_i'u_j'} = f\overline{(u_i'u_j')}_{\text{BousinesqTransition}} + (1-f)\overline{(u_i'u_j')}_{\text{RSM}} \qquad (3)$$

The Reynolds stress tensor $\overline{(u_i'u_j')}_{\text{RSM}}$ represents the solution of the 'turbulent' Reynolds stress transport equation of the previously introduced RSM. The Reynolds stress tensor $\overline{(u_i'u_j')}_{\text{Boussinesq-Transition}}$ is obtained by applying an associated transition model. This transition model uses the theory of laminar kinetic energy dynamics, which is implemented into an eddy-viscosity model (Walters & Cokljat, 2008). To improve the numerical stability, the weighting factor f is set to a constant value of 0.4, (Maduta *et al.*, 2018). This model scheme is designed to predict laminar-to-turbulent transition, rather than to modify the RSM equations explicitly in a term-by-term manner.

Compared to the baseline RSM, the eddy-resolving IIS-RSM (Jakirlić & Maduta (2015) and Jakirlić & Maduta (2016)) accounts for an additional production term, which is introduced into the transport equation, governing the specific dissipation rate ω^h

$$\left(\frac{D\omega^h}{Dt}\right)_{IIS-RSM} = \left(\frac{D\omega^h}{Dt}\right)_{RSM} + P_{IIS-RSM} \qquad (4)$$

The idea of this modification is based on the SAS (Scale-Adaptive Simulation) methodology, which was originally proposed by Menter & Egorov (2010), in conjunction with the popular $k-\omega-SST$ model of turbulence. The production term $P_{IIS-RSM}$

$$P_{IIS-RSM} = 0.003 * max\left[29.1\left|\frac{\partial^2\overline{u_i}}{\partial^2 x_j}\right|\sqrt{k} - 40T_2, 0\right] \qquad (5)$$

increases the specific dissipation rate locally around the separating region and in the separated shear layer, causing a suppression of the modelled kinetic energy of turbulence towards the residual motion level. It is important to notice that the equation (5) does not explicitly depend on the von Karman length scale, as previously applied in Jakirlić & Maduta (2015) and Jakirlić & Maduta (2016), but solely on the second derivative of the underlying velocity field. The resulting model is consequently a grid-spacing free formulation adjusting to the scales residing in the unresolved residual motion, by interplaying with the underlying grid resolution. Herewith, the development of fluctuating turbulence is enabled. Due to the grid-spacing free formulation the IISRSM can be described as a second generation unsteady RANS model according to Fröhlich & Von Terzi (2008). In addition, for the sake of comparative analysis, all computational results are compared with the results of a pure laminar computation.

RESULTS AND DISCUSSION

In this section, the numerical results are comparatively assessed to the experimental MRV data. The phase-averaged MRV measurements include 36 time steps corresponding to a temporal resolution of $72.8ms$. The numerical simulations are analyzed at the same times as the MRV data. The first step is a comparison between the experimentally and numerically obtained velocity fields. Fig. 5 illustrates the structural properties of the velocity field, detected at four characteristic times, corresponding to the maximum acceleration (occurring at the highest Reynolds number observed, $Re = 3200$), maximum deceleration (characterized by flow reversal), second acceleration peak (corresponding to $Re \approx 400$) and the flow relaxation phase featured by a plateau indicating zero velocity. It is important to notice that shortly after the maximum volume flow rate is reached, the flow deceleration consequently leads to a separation of a toroidal eddy (time instant 2, Fig. 5). Afterwards, this eddy travels over the time of one cardiac cycle to the proximal downstream ending of the aneurysm. The separated eddy forms a region of transitional to low-intensity turbulent flow which barely interacts with the aneurysm walls. All numerical models are capable of capturing this important flow phenomena so that the computational results exhibit close agreements with the measurements.

The temporal evolution of the dimensionless mean velocity profile over the cross sections corresponding

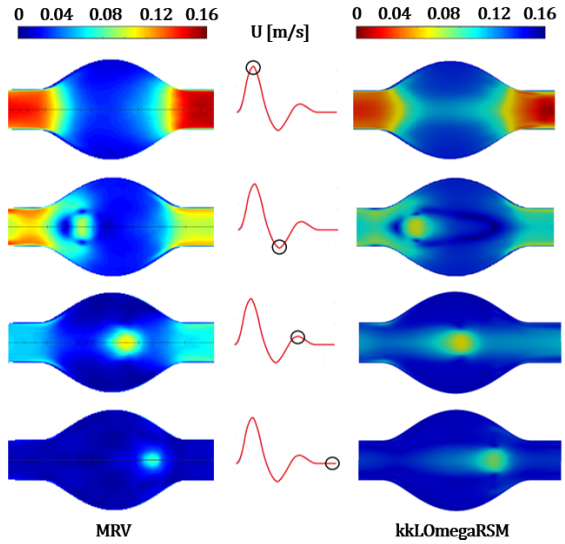

Figure 5. Velocity fields (magnitude) at four characteristic times within the aneurysm model obtained experimentally (left) and computationally (right) during one physiological pulsating cycle.

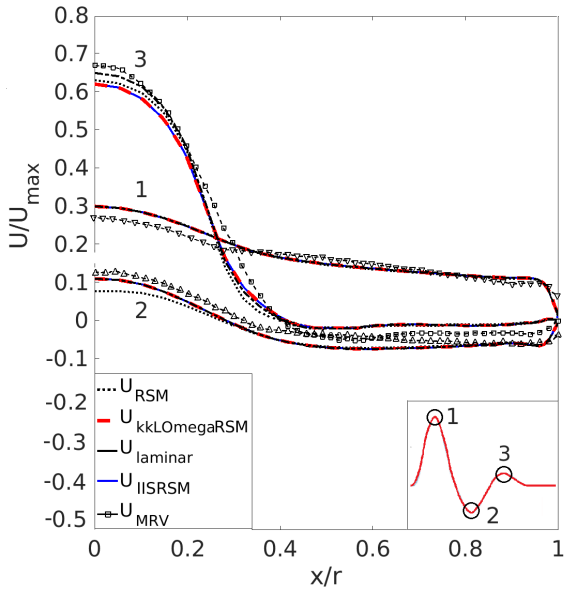

Figure 6. Velocity profiles at the middle line of the generic aneurysm at three characteristic times over the dimensionless aneurysm radius x/r.

to the middle of the aneurysm section, offers a more detailed quantitative comparison between experimental and computational results (Fig. 5). The velocity profile shapes reflect relevant flow modifications caused by accelerating and decelerating phases. Due to the limited spatial resolution, the MRV data itself may contain an uncertainty with the consequence that the corresponding velocity profiles cannot be interpreted as the ground truth velocity profiles. Nevertheless, the results exhibit a close mutual agreement of the experimental and numerical data over a larger portion of the pulsating cycle.

Figure 7 shows a comparison of the experimental and numerical dimensionless wall shear stress distribution over the entire length of the generic aneurysm ($-2 \leq z/d \leq 2$). The WSS τ is made dimensionless by the maximum WSS τ_0 captured at the healthy segment of the generic aorta ($z/d \leq -2$). All results show a highly dynamic spatial and

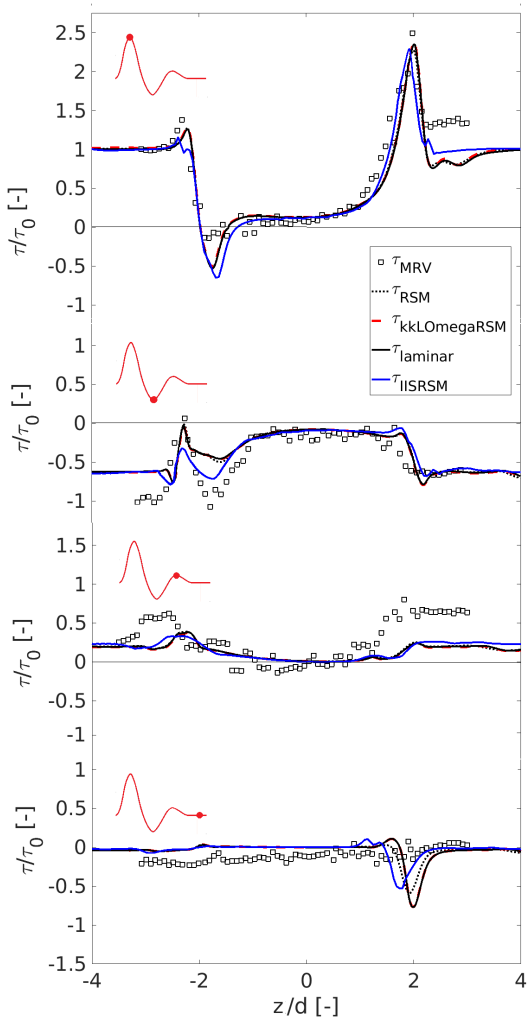

Figure 7. Temporal evolution of the numerical and experimental wall shear stress distribution of the pulsatile aneurysm flow over a cardiac cycle.

temporal evolution at the beginning ($z/d \approx -2$) and at the end ($z/d \approx 2$) of the aneurysm. At the point of the maximum diameter of the aneurysm ($z/d \approx 0$), the WSS varies slightly over a cardiac cycle and is constantly close to zero. The maximum load on the walls hereinafter emerge especially on the proximal endings of the generic AAA and are closely related to the corresponding volume flow rate. It is important to notice, that all numerical results, apart from a few exemptions, follow the laminar solution. This condition indicates, like in the case of the previously illustrated velocity fields in Fig. 5, a weakly turbulent flow behavior. This flow regime is characterized by a smaller perturbation of the velocity amplitude over the entire cycle, affecting

only marginally the laminar-like mean flow structure. All numerical results show a good correspondence to the experimental MRV data. However, there are some minor differences in the WSS evolution. The first noticeable difference in the WSS can be seen at the time of maximum back flow at the beginning of the aneurysm (Fig. 7, second time instant). The MRV WSS data shows a sharp negative peak at this position, which indicates a transitional flow separation. However, the computational results at this point and time differ from each other as well as from the experimental data. The eddy-resolving IIS-RSM captures for example the very beginning of the laminar-turbulent transition but does not show that sharp peak as the experimental data does. Due to the short duration of the flow separation at this time instant, two other RANS models result in a laminar-like solution. The second difference is the high wall shear stress value at the proximal beginning and ending of the aneurysm during the third time sequence which is shown in Fig. 7. These unusually high MRV WSS values may be the result of turbulent flow regimes which are not correctly captured by the numerical simulations, or the consequence of possible measurement errors due to limited temporal and spatial resolutions. The experimental WSS data at the fourth time instant, which is characterized by a zero volume flow rate, also show an unexpected behaviour. Despite the absence of a flow it is noticeable that the MRV WSS data starts with negative values, showing subsequently a slight increasing progression over the aneurysm. These irregularities may be an indicator for possible measurement errors or unidentified secondary flow motion. The numerical simulations capture the influence of the separating toroidal eddy on the WSS, related to the time instant 2. A corresponding behaviour of the MRV WSS data cannot be seen.

CONCLUSION AND OUTLOOK

The present numerical study provides a comparative analysis between experimentally and numerically obtained transient velocity fields, as well as the temporal evolution of wall shear stresses of a pulsatile flow inside a generic aortic aneurysm. All numerical results show a close correspondence to the experimental MRV data. The investigated pulsatile aneurysm flow is of a weakly turbulent transitional nature. Due to the weak wall interaction within the transitional flow regimes, the numerically obtained WSS values follow mainly a laminar-like behaviour. All results show a highly dynamic behaviour at the diverging beginning and at the converging end of the aneurysm. The maximum WSS values, representing an important factor for controlling the aneurysm growth, also occur in this regions. The numerical study also identified regions of uncertain WSS behaviour so that this regions can be further investigated by Laser Doppler Anemometry (LDA). Important future goal of the present investigation is to use the combined experimental and computational results aiming at refining the sparse MRV data by applying a variational data assimilation technique.

Acknowledgements. The financial support of the German Research Foundation (DFG) (Grant number TR 194/56-1) is gratefully acknowledged. The authors would like to thank the Lichtenberg HPC at TU Darmstadt for the computing time.

REFERENCES

Bauer, A., Wegt, S., Bopp, M., Jakirlić, S., Tropea, C., Krafft, A.J., Shokina, N., Hennig, J., Teschner, G. & Egger, H. 2019 Comparison of wall shear stress estimates obtained by laser Doppler velocimetry, magnetic resonance imaging and numerical simulations. *Experiments in Fluids* .

Fröhlich, J. & Von Terzi, D. 2008 Hybrid LES/RANS methods for the simulation of turbulent flows. *Progress in Aerospace Sciences* **44** (5), 349–377.

Jakirlić, S. & Hanjalić, K. 2002 A new approach to modelling near-wall turbulence energy and stress dissipation. *Journal of Fluid Mechanics* **459**, 139–166.

Jakirlić, S. & Maduta, R. 2015 Extending the bounds of steadyRANS closures: Toward an instability-sensitive Reynolds stress model. *International Journal of Heat and Fluid Flow* **51**, 175–194.

Jakirlić, S. & Maduta, R. 2016 Sensitized-RANS modelling of turbulence: Resolving turbulence unsteadiness by a (near-wall) Reynolds stress model. In *Progress in Wall Turbulence 2*, pp. 17–35. Springer.

Kaufman, J., Geller, SC, Petersen, MJ, Cambria, R_P, Prince, MR & Waltman, AC 1994 MR imaging (including MR angiography) of abdominal aortic aneurysms: comparison with conventional angiography. *AJR. American Journal of Roentgenology* **163** (1), 203–210.

Lasheras, J. C. 2007 The biomechanics of arterial aneurysms. *Annu. Rev. Fluid Mech.* **39**, 293–319.

Maduta, R., Wegt, S. & Jakirlic, S. 2018 A transition-sensitive Reynolds-stress model of turbulence. In *12th Int. ERCOFTAC Symp. on Engineering Turbulence Modelling and Measurements (ETMM12)*. Montpellier, France, September 26-28.

Mao, S., Ahmadi, N., Shah, B., Beckmann, D., Chen, A., Ngo, L., Flores, F. R, lin Gao, Y. & Budoff, M. J. 2008 Normal thoracic aorta diameter on cardiac computed tomography in healthy asymptomatic adults: impact of age and gender. *Academic Radiology* **15** (7), 827–834.

Menter, FR & Egorov, Y 2010 The scale-adaptive simulation method for unsteady turbulent flow predictions. part 1: theory and model description. *Flow, Turbulence and Combustion* **85** (1), 113–138.

Petersson, S., Dyverfeldt, P. & Ebbers, T. 2012 Assessment of the accuracy of mri wall shear stress estimation using numerical simulations. *Journal of Magnetic Resonance Imaging* **36** (1), 128–138.

Salsac, A-V, Sparks, SR, Chomaz, J-M & Lasheras, JC 2006 Evolution of the wall shear stresses during the progressive enlargement of symmetric abdominal aortic aneurysms. *Journal of Fluid Mechanics* **560**, 19–51.

Vorp, David A, Raghavan, ML & Webster, Marshall W 1998 Mechanical wall stress in abdominal aortic aneurysm: influence of diameter and asymmetry. *Journal of Vascular Surgery* **27** (4), 632–639.

Walters, D K. & Cokljat, D. 2008 A three-equation eddy-viscosity model for reynolds-averaged navier–stokes simulations of transitional flow. *ASME Journal of Fluids Engineering* **130** (12), 121401.

Womersley, J. R. 1955 Method for the calculation of velocity, rate of flow and viscous drag in arteries when the pressure gradient is known. *The Journal of Physiology* **127** (3), 553–563.